

Hydrodynamic and Colloidal Interactions in Concentrated Charge-Stabilized Polymer Dispersions

F. M. Horn,^{*} W. Richtering,^{*,1} J. Bergenholtz,[†] N. Willenbacher,[‡] and N. J. Wagner[§]

^{*}Institute for Macromolecular Chemistry, University of Freiburg, Stefan-Meier Strasse 31, D-79104 Freiburg, Germany; [†]Department of Physical Chemistry, Göteborg University, 412 96 Göteborg, Sweden; [‡]Polymers Laboratory, BASF Aktiengesellschaft, D-67056 Ludwigshafen, Germany; and

[§]Center for Molecular and Engineering Thermodynamics, Department of Chemical Engineering, University of Delaware, Newark, Delaware 19716

Received September 1, 1999; accepted December 28, 1999

Hydrodynamic and colloidal interactions are explored in concentrated, charge-stabilized colloidal dispersions by measuring the dependence of rheology (e.g., low and high-shear viscosity, high-frequency viscosity, and modulus) and self-diffusivity on salt content, particle size, and concentration. Model, sulfonated polystyrene latices of varying diameter are prepared and investigated by shear rheology, high-frequency torsional resonance, electrophoresis, titration, and dynamic light scattering. The high-frequency and high-shear viscosity both are dominated by hydrodynamic interactions, but are shown not to be identical, due to the microstructure distortion resulting from high shear rates. The short-time self-diffusion is also shown to be insensitive to direct particle interactions, but has a different concentration dependence than the high-frequency viscosity, further illustrating a predicted violation of a generalized Stokes–Einstein relationship for these properties. The apparent colloidal surface charge is extracted from the high-frequency elastic modulus measurements on concentrated dispersions. The surface charge is in good agreement with results from critical coagulation concentration measurements and perturbation theories, but disagrees with electrophoretic mobility experiments. This indicates that the effective surface charge determined by torsional high-frequency measurements is a more reliable predictor of the salt stability of charge-stabilized dispersions, in comparison to ζ -potentials determined from electrophoretic mobilities. Further, we demonstrate by direct comparison that measurements of the apparent plateau modulus by rotational rheometry underestimate the true, high-frequency modulus and provide unreliable estimates for the surface charge.

© 2000 Academic Press

Key Words: charge stabilized dispersions; polymer latex; surface charge; torsional resonance; FOQELS; short-time self-diffusion; high-frequency modulus; high-frequency viscosity; zeta-potential.

1. INTRODUCTION

The rheological properties of concentrated colloidal dispersions (latices) are determined by the interplay between direct particle–particle interactions and hydrodynamic interactions.

¹To whom correspondence should be addressed. E-mail: rich@uni-freiburg.de.

Stabilizing colloidal systems by electrostatic particle–particle repulsion introduced either by the initiator, appropriate comonomers, or ionic surfactants is a widely used strategy. In this case the interaction potential depends on the charge density on the particle surface as well as on the electrolyte concentration (ionic strength) of the continuous phase. Manipulating colloid stability, phase behavior and rheology for aqueous based systems requires an accurate assessment of surface charge. Environmental driving forces and market competition are pushing formulators toward aqueous suspension of ever more complex particles and particle–surfactant–polymer mixtures and to increased particle loadings. Consequently, a reliable, robust, and accurate method for determining colloidal surface charge is critical for predicting dispersion performance. Extracting this quantity from shear rheology measurements requires substantial modeling, which includes assumptions about the dispersion microstructure and models for the hydrodynamic contribution to the particle stress (see, for example, Buscall (1, 2), Wagner and Klein (3), and Brady (4)), which can make the method complicated and ambiguous.

In contrast to steady shear and low-frequency oscillatory shear, much less is known about the response of charge-stabilized dispersions to high-frequency oscillatory shear. High frequency is defined relative to the Brownian (diffusive) relaxation time of the particles in the dispersion. Applying such an oscillating shear stress with low amplitudes, the structure of the dispersion cannot relax by particle diffusion during the cycle. Thus, η'_{∞} should directly depend on hydrodynamic interactions only; thermodynamic forces (i.e., interparticle forces and Brownian motion) enter only indirectly into η'_{∞} as they determine the colloidal microstructure. Consequently, stable liquid dispersions without flocculation should show similar high-frequency viscosities largely independent of the nature and strength of the interparticle forces, such that η'_{∞} for charge-stabilized latices should behave similar to that of hard-sphere systems.

The high-frequency viscosity η'_{∞} of hard-sphere systems has been intensively studied by van der Werff *et al.* (5). The concentration dependence of η'_{∞} follows a mastercurve independent of particle size and is well described by theoretical predictions

of Beenakker (6). Blom *et al.* (7) investigated a charge stabilized PS latex at different ionic strengths and found convergence of $\eta'_\infty(\omega)$ when the frequency ω was increased up to 2.5 kHz, indicating that η'_∞ was measured at sufficiently high frequencies. Further results for near hard-sphere systems are provided by Shikata and Pearson (8), who employed time-temperature superposition to reach high enough frequencies with a conventional rheometer. The high-frequency rheology of hard spheres has been discussed in detail by Lionberger and Russel (9).

Another important dynamic property of colloidal dispersions closely related to the suspension shear viscosity is the particle mobility. Starting from the well-known Stokes-Einstein equation relating the diffusivity of suspended particles to the shear viscosity in the dilute particle limit, researchers are looking for extensions of this relationship to dense colloidal systems for both academic and practical reasons (10). The dynamics of concentrated dispersions are not simply described by a single diffusion coefficient or viscosity, consequently the time-scale on which both quantities are compared has to be carefully considered. Imhof *et al.* (11) determined the long-time self diffusion coefficient of concentrated, charge-stabilized dispersions and found a similar, but not identical, concentration dependence as that of the reciprocal zero-shear viscosity ($1/\eta_0$). Recently Segré *et al.* (12) investigated an index-matched hard-sphere system by dynamic light scattering (QELS) and observed that the concentration dependence of the collective diffusion coefficient measured at the peak (q_{\max}) of the structure factor $S(q)$ was identical to that of the zero-shear viscosity η_0 (see also (13)); here, q denotes the magnitude of the scattering vector.

Single particle motion in a concentrated dispersion is experimentally observed to exhibit diffusive motion at both short and long times characterized by short- and long-time self-diffusion coefficients, respectively. The former arises due to small displacement motion localized in the essentially static cage of nearest neighbor particles, while the latter results from the particles exploring many statistically independent environments of neighboring particles over a much longer time scale. Thus, the short time motion is only affected by the hydrodynamic interactions, which propagate through the solvent as steady interactions on this time scale. The additional drag force results from the solvent motion generated by the diffusing particles “scattering” off of the other particles present in solution. Interparticle forces enter into the determination of the short-time diffusivity only indirectly in determining the microstructure of the fluid. At longer times the motion is also retarded by the interparticle interactions between the diffusing particles. Conceptually, the interparticle forces serve to strengthen the “cage” that surrounds each particle in the fluid.

In comparing diffusion and viscosity one might expect that η'_∞ and D_s^s are closely related, both depending on hydrodynamic quantities only. Upon closer inspection, however, there is no theoretical basis for a simple correlation between both quantities. η'_∞ is related to the dissipation generated by an externally applied bulk, oscillatory shear field, while D_s^s is governed by

the dissipation resulting from a flow generated by a diffusing particle.

For hard-sphere systems, Beenakker and Mazur (14) provided theoretical descriptions for the short-time behavior. Indeed, they predicted a slightly weaker concentration dependence for D_s^s as compared to η'_∞ (6). This is in accordance with results from computer simulations (15, 16) and dilute limiting hard-sphere expansions (17–19). In contrast to these theoretical predictions, studies on hard-sphere systems by Shikata and Pearson (8) and Zhu *et al.* (20) came to the conclusion that a generalized Stokes-Einstein relation (Eq. [1]) holds within experimental accuracy:

$$D_s^s(\phi) = k_B T / (6\pi \eta'_\infty(\phi) a). \quad [1]$$

This comparison is not unambiguous, however, as Shikata and Pearson compared the results from different hard-sphere systems and Zhu used the many-body hard sphere theory by Beenakker (6) for η'_∞ for comparison with the experimental diffusion data.

Methods for determining both D_s^s (21, 22) and η'_∞ (23) accurately for concentrated, stable colloidal dispersions are now established, enabling rigorous exploration of the relationship between short-time self-diffusion and the high-frequency viscosity. Establishing this relationship quantitatively is important in the modeling of concentrated colloidal dispersions (4) as well as the interpretation of rheo-optical methods such as diffusing wave spectroscopy (10, 24). In a previous letter (25) we demonstrated for a charge stabilized latex at high colloid concentrations in the liquid phase that there is a measurable difference between these quantities that can be quantitatively described by theories including many-body hydrodynamic interactions. One goal of this paper is to expand upon that observation.

High-frequency viscoelastic measurements are also a valuable method for characterizing interparticle forces, as previously demonstrated by a number of researchers (23, 26, 27). Through statistical mechanics, the elastic response can be directly related to the interparticle forces. With a suitable approximation for the liquid phase microstructure, these high-frequency viscoelasticity measurements can be interpreted and quantified as interparticle potentials (23, 28). Bergenholtz *et al.* (23) presented a robust model for the extraction of the effective surface potentials from G'_∞ for concentrated charge-stabilized dispersions with liquid-like structure. Since most of the methods commonly used to characterize the surface charge of colloidal particles require diluted samples, high-frequency rheology provides a valuable new method for an *in situ* characterization of concentrated dispersions with respect to interparticle interactions.

Bergenholtz *et al.* studied relatively small particles (diameter ca. 80 nm) at fairly high salt concentrations of $[KCl] \geq 10$ mM KCl and found good agreement for surface charge densities as compared with results from electrophoresis. In this study, model polystyrene latices were synthesized and investigated with the same experimental setup in order to determine the applicability of this new method over a broader range of particle sizes, surface charges, and salt concentration. We also compare with

electrophoretic mobility and critical coagulation concentration measurements, which are often used for determining the surface charge.

2. EXPERIMENTAL

Monodisperse poly-(styrene) (PS) dispersions were prepared by soap-free emulsion polymerization using potassium persulfate (KPS, Merck) as the initiator. Styrenesulfonate potassium salt (4-vinylbenzenesulfonic acid potassium salt, Fluka 85–95%) was added as comonomer, leading to strong acidic sulfonate groups on the particle surface of a comparable dissociation constant with respect to the sulfate groups resulting from initiator decomposition.

Emulsion polymerization was carried out at 80°C in a 2-L three-neck flask under nitrogen atmosphere using pure water (Milli-Q grade) as the reaction medium. Styrene (Fluka, >99%, stabilized with 0.005% 4-*tert*-butylcatechol) was used without further purification. Variation of particle size was achieved by adjusting the quantities of comonomer and initiator and using bivalent cations in small amounts to gain control over particle size and surface charge. The dispersion (~15% by weight) was filtrated three times through glass wool to remove coagulate.

Soluble by-products in the serum were removed by dialysis (dialysis tube, Nadir, Roth; pore size, 25–30 Å) against pure water (Milli Q grade) until the conductivity of the dialyzate remained below 10 $\mu\text{S}/\text{cm}$ for several days.

Concentrated dispersions were stored in KCl solutions of defined ionic strength and dialysis was continued until the conductivity of the dialyzate remained constant at the target value. Concentration series were prepared by diluting the dispersions with the KCl solutions used as dialyzate. Gravimetrically determined weight fractions were converted to volume fractions using a density of 1.05 g/mL for the PS particles.

Particle size and size distribution were determined from transmission electron microscopy (TEM) (Philips, 100 kV acceleration voltage). The latex samples were prepared on a copper grid, coated with a thin carbon film. Each micrograph, showing up to 50 particles, was sent via a CCD camera (SIT 66) to a digital image processing unit (KONTON, IBAS) and 500–600 particles/sample were counted. Polydispersity was defined as the standard deviation (stdev.) of the particle size with respect to the average particle size. These particle sizes were confirmed by tapping-mode atomic force microscopy. For each sample large crystalline hexagonal structures without structure defects could be found on the surface of dried latex films, prepared on polished silicon wafers. The particle diameter was determined by measuring the lateral dimension of a single strand of 30 to 70 particles.

Conductometric titrations of the acidic surface groups were done by an automatic titrator (Schott, TR600) using KOH solution (0.001 mol/L) as titrant. First the dispersions were treated three times with a mixture of anionic and cationic ion-exchange resin (Amberlite IR120, strong acidic, Amberlite IRA 430 strong

basic) for 1–2 days. Before and during titration, the diluted dispersions were purged thoroughly with nitrogen to prevent absorption of carbon dioxide from air.

Electrophoretic mobilities were determined by a Malvern Zetamaster 3 (Malvern Instruments, GB) for a range of salt concentrations at neutral pH. Ten runs were performed on each sample.

Determination of the critical coagulation concentration (ccc) was done by preparing KCl-dilution series from 100 to 800 mM and adding latex to give samples of 0.2% by weight. These dispersions were stored in sealed tubes for 10 days at room temperature. Flocculation of the samples could be detected easily by eye as the change of the turbidity of the samples and/or occurrence of large latex-flocs. Uncertainty of this method concerning the ccc was $[\text{KCl}] = \pm 20 \text{ mM}$.

Diffusion coefficients D_0 in dilute solution were measured by means of quasi-elastic light scattering using an ALV goniometer and an ALV 5000 correlator at scattering angles between 30° and 120°. The samples were diluted to 10⁻⁶ g/ml before measurements. D_0 was calculated from the single exponential autocorrelation function (ACF) by cumulant analysis (29).

Fiber optical quasi-elastic light scattering (FOQELS) measurements were performed with a self-built device. Details of the experimental setup are described by Wiese and Horn (22, 30). The beam of a He-Ne laser ($\lambda_0 = 632.8 \text{ nm}$) (scattering vector $q_{\text{exp}} = 0.0268 \text{ nm}^{-1}$) is coupled into a single mode fiber (core diameter 4 μm , cladding 125 μm , numerical aperture 0.1) and enters a four-door coupler by pigtail 1. The light leaves the coupler via pigtails 2 and 4, and the optodes are immersed into the concentrated polymer dispersion and an index matching fluid (toluene), respectively. In order to extend the experimental scattering vector q_{exp} to larger values, a second setup with shorter wavelength was built. Using an argon-ion laser and a corresponding single mode fiber (core diameter 3 μm , cladding 125 μm , numerical aperture 0.1) we employed the lines at $\lambda_0 = 457.9 \text{ nm}$ ($q_{\text{exp}} = 0.0366 \text{ nm}^{-1}$) and $\lambda_0 = 514 \text{ nm}$ ($q_{\text{exp}} = 0.0327 \text{ nm}^{-1}$).

The optodes were prepared in the way described by Wiese and Horn, i.e., they were ground at a slant angle of about 10° in order to avoid heterodyning effects from reflection of the primary beam (22). The backscattered light reaches the photomultiplier via pigtail 3. The time autocorrelation function (ACF) was calculated by a multiple- τ ALV-5000 correlator (ALV-Langen). Ten independent measurements were performed on every concentration of each sample and put together to an averaged ACF. The ACFs of higher concentrated samples showed a nonexponential decay, so D_s^\ddagger was calculated from the averaged ACF by a second-order cumulant analysis (29) of correlator-channel 7-70 (28–280 μs).

The criterion for measuring D_s^\ddagger is confined by q_{exp} being larger than q_{max} at the maximum of the structure factor $S(q_{\text{max}})$. The product $q_{\text{exp}} \times a$, with a denoting the particle radius, should be much larger than 2 when D_s^\ddagger is to be probed (31). FOQELS measurements on sample PS200 were performed using light of $\lambda_0 = 458 \text{ nm}$, $\lambda_0 = 514 \text{ nm}$, and $\lambda_0 = 633 \text{ nm}$. Results for each wavelength were equivalent, ensuring that self-diffusion was

probed. For PS120 D_s^s was not determined because the criterion for probing the short-time self-diffusion could not be fulfilled by the FOQELS setup.

High-frequency shear experiments were performed using a commercially available torsional resonator (Rheoswing, Physica) described in detail in a previous paper (23). The resonance characteristic of the piezoelectrically driven stainless steel cylindrical rod changes upon immersion into a fluid. The resonance frequency ω_0 is lowered and the width $\Delta\omega$ of the resonance curve increases due to the viscoelastic properties of the surrounding fluid.

The complex mechanical impedance $Z^* = R + iX$ of the liquid is related to the damping and the frequency shift according to the following:

$$R = K_1(\Delta\omega_{\text{sample}} - \Delta\omega_{\text{air}}) \quad [2]$$

$$X = K_2(\omega_{0,\text{sample}} - \omega_{0,\text{air}}) \quad [3]$$

To experimentally measure the limiting high-frequency viscosity the resonance frequency (ω) must be larger than the characteristic frequency D_s^s/l^2 of the dispersion (32, 33) $\omega/2\pi \gg D_s^s/l^2$, with D_s^s the short-time self-diffusion and l the mean interparticle separation. The Rheoswing operates at a resonance frequency of 8858 Hz in air which is truly in the high frequency limit for aqueous dispersions with radii larger than 100 nm (23). For sample PS120 the characteristic frequency, calculated with D_0 taken as D_s^s , is approx. 1 kHz. For higher concentrated dispersions D_s^s decreases and so the inverse structural relaxation times become less than 1 kHz. The mechanical quality factor $\omega_0/\Delta\omega$ of the resonator is about 2000 at 20°C. The penetration depth δ of the shear wave propagating from the resonator's surface into the liquid is 6 μm in water and about 50 μm for the most concentrated dispersions investigated here. Since $\delta \gg a$, bulk properties of the dispersion are probed. Further, as δ is much smaller than the radius of the rod, the plane wave approximation applies and the real and imaginary part of the shear modulus are related to the mechanical impedance via $G' = (R^2 - X^2)/\rho$ and $G'' = 2RX/\rho$.

The instrument constants $K_1 = 76 \text{ kg/m}^2$ and $K_2 = 95 \text{ kg/m}^2$ are obtained from calibration measurements on a series of Newtonian liquids ($G' = 0$, $\eta = \eta'_\infty = G''/\omega$) covering the viscosity range from 1 to 10 mPas.

The penetration depth δ is large compared to the oscillation amplitude α of the rod ($\alpha \approx 50 \text{ nm}$ according to the manufacturer). Accordingly, the maximum strain $\gamma = \alpha/\delta$ is below 0.01 and thus linear viscoelastic properties of the dispersions are probed (34).

An RFSII rheometer (Rheometrics) was used to determine zero-shear viscosities from the low-shear plateau in steady shear experiments using a Couette shear cell (cup diameter, 34 mm; bob diameter, 32 mm; bob height, 36.4 mm). Low-frequency oscillation experiments, determination of high-shear viscosity, and checking the reproducibility of low-shear flow curves were performed on a controlled stress rheometer (Bohlin CVO) and

cone/plate tools (CP 4°/40 mm, 1°/40 mm). All measurements were conducted at 20°C.

3. RESULTS AND DISCUSSION

3.1. Particle Characterization

Three samples of different particle sizes were studied at electrolyte concentrations [KCl] of 10, 1, and 0.1 mM for Latex PS200 and PS310 and 50, 10, and 1 mM for Latex PS120. Table 1 summarizes the results from particle characterization. Quasi-elastic light scattering (QELS), transmission electron microscopy (TEM), and atomic force microscopy (AFM) all revealed a low size polydispersity. The variation of D_0 with salt content was less than 2%, and no systematic trend was observed, pointing to an absence of partial electrosteric stabilization characteristics (hairy layer) or swelling of the particle dimensions on changing ionic strength. The number of surface charges per particle were determined by conductometric titration. The results are listed also in Table 1. Titration curves consisted of two linear branches. Only one point of equivalence could be found, demonstrating the exclusive presence of strong acidic sulfate and sulfonate groups on the particle surface (35, 36). There was no indication for carboxylic groups created by the so-called Kolthoff reaction (37) during synthesis.

The electrophoretic mobilities were measured for each particle size and salt content using highly diluted samples. Electrophoretic mobilities strongly depended on ionic strength and decreased with decreasing salt content. This so-called atypical electrophoretic mobility behavior is often observed for charged polystyrene (PS) particles. Others have reported that the mobility goes through a maximum at moderate salt content of ca. 10–50 mM KCl (36, 38). These observations are commonly explained by specific ion adsorption (39) or a hairy-layer model (40). A new model, based on the theory of O'Brien and White (41), was recently presented by Antonietti and Vorwerg (38) and explained the atypical mobility behavior by relaxation processes of the electric double layer without any further assumptions like specific ion adsorption. Note that variations of the pH between 4 and 9 did not lead to significant changes in the electrophoretic mobility. This is another indication that the surface charge originates only from strong acid groups.

TABLE 1
Properties of the Monodisperse Latices

	PS120	PS200	PS310
Diameter (QELS, nm)	120	200	310
Diameter (TEM, nm)	107	192	291
Polydispersity (SD)	8%	4%	6%
Diameter (AFM, nm)	113	198	296
q^a ($\mu\text{C}/\text{cm}^2$)	9	6.3	7.7
ccc KCl (mol/L) ^b	0.44	0.32	0.32

^a Surface charge density determined by conductometric titration.

^b ccc, critical coagulation concentration.

TABLE 2
Electrophoretic Mobilities (Elec-mob) and Surface Potentials Calculated According to Henry (42) and O'Brien-White (41)

[KCl] (mmol/L)	PS120			PS200			PS310		
	Elec-mob ($10^8 \text{ m}^2 \text{ V}^{-1} \text{ s}^{-1}$)	ψ_s^a (mV)	ψ_s^b (mV)	Elec-mob ($10^8 \text{ m}^2 \text{ V}^{-1} \text{ s}^{-1}$)	ψ_s^a (mV)	ψ_s^b (mV)	Elec-mob ($10^8 \text{ m}^2 \text{ V}^{-1} \text{ s}^{-1}$)	ψ_s^a (mV)	ψ_s^b (mV)
50	-5.1 ± 0.82	-79	-84						
10	-4.78 ± 0.08	-76	-100	-5.18 ± 0.18	-81	-106	-5.97 ± 0.07	-92	-114
1	-3.58 ± 0.24	-64	-68	-3.69 ± 0.56	-60	-70	-4.18 ± 0.17	-68	-73
0.1				-3.26 ± 0.09	-60	-66	-3.45 ± 0.08	-63	-78

^a ψ_s calculated according to Henry.

^b ψ_s calculated according to O'Brien-White.

Conversion of electrophoretic mobilities to ζ -potentials requires a theoretical model, the choice of which depends on the conditions of the experiment and the sample. Only in the limit of large $\kappa \cdot a$ or small $\kappa \cdot a$, with κ the inverse Debye length and a the particle radius, corresponding to very large particles with thin double layers or very small particles with very thick double layers are the simple expressions of Smoluchowski and Debye-Hückel valid, respectively. For intermediate $\kappa \cdot a$ values and rather small surface potentials of ca. -25 mV, the ζ -potential can be calculated by Henry's equation (42). Our latex systems, however, were in a range of $\kappa \cdot a$ between 5 and 50 and had absolute surface potential values higher than -25 mV, so Henry's equation is not strictly valid. For high surface potentials, the theory of O'Brien and White (41) should hold. Both theories were used to calculate ζ -potentials and results are listed in Table 2.

The zero-shear viscosity and high-shear viscosity were determined from the low- and high-shear Newtonian plateaus observed in the steady shear flow curves. Both plateaus were experimentally accessible so that no extrapolations were necessary. The normalized zero-shear viscosities $\eta_{0,r} = \eta_0/\mu$ and high-shear viscosities $\eta_{\infty,r} = \eta_{\infty}/\mu$ for PS200 are shown in Fig. 1

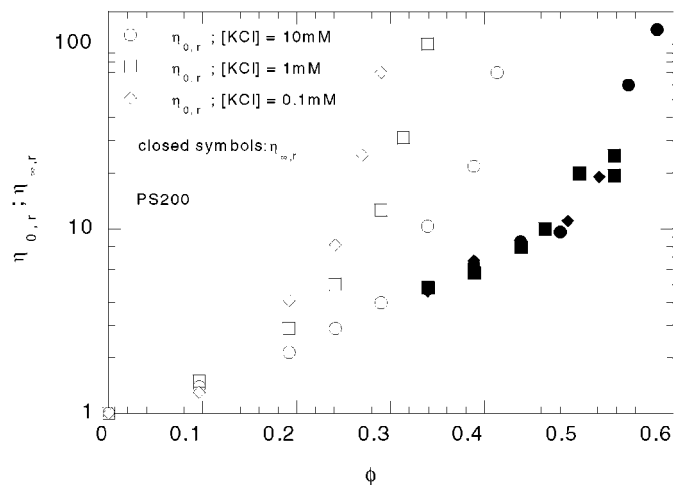


FIG. 1. Comparison of $\eta_{0,r} = \eta_0/\mu$ (open symbols) and $\eta_{\infty,r} = \eta_{\infty}/\mu$ (filled symbols) for PS200 at different salt contents of 10 mM (○, ●), 1 mM (□, ■), and 0.1 mM (◇, ◇).

as a function of volume fraction. Here μ represents the viscosity of the dispersion medium, water. The zero-shear viscosities (η_0) diverge at volume fractions, denoted as ϕ_{\max} , which are well below values of 0.58–0.63, typical for hard spheres. Furthermore, ϕ_{\max} strongly depends on the ionic strength which determines the range of electrostatic interactions. In contrast the high-shear viscosity is essentially independent of salt concentration, depending only on volume fraction.

An estimate of the extra excluded volume due to the electrical double layer can be obtained from the point of the viscosity divergence. We take the diverging viscosity to be described by the Quemada equation (43),

$$(\eta_0/\mu) = (1 - \phi/\phi_{\max})^{-2}, \quad [4]$$

which is frequently used to describe the zero-shear viscosity of concentrated hard-sphere dispersions. The exponent of -2 in Eq. [4] has also been proposed in theoretical work by Brady (4). The ϕ_{\max} values tabulated in Table 3 were determined from the intercept of the abscissa in a plot of $(\eta_0/\mu)^{-0.5}$ vs volume fraction, as shown in Fig. 2. Only the highest volume fractions were included in this analysis.

The relative contribution of the electrostatic repulsion to the effective excluded volume of the dispersion increases with decreasing particle size. For the smallest particles (PS120) the zero-shear viscosity diverged at a volume fraction of 0.31 at [KCl] = 0.1 mM compared to 0.39 found for PS310 at [KCl] = 0.1 mM

Effective radii a_{eff} can be calculated from Eq. [5], which compares the experimentally determined ϕ_{\max} with $\phi_{\max, \text{HS}}$, the maximum packing fraction of hard-sphere suspensions. The

TABLE 3
 $\phi_{\max, \text{exp}}$ Values Determined from Zero-Shear Viscosity Data for the Three Different Particle Sizes at Different Salt Contents

[KCl] (mM)	PS120	PS200	PS310
50	0.5	—	—
10	0.433	0.465	0.493
1	0.383	0.37	0.436
0.1	0.31	0.328	0.39

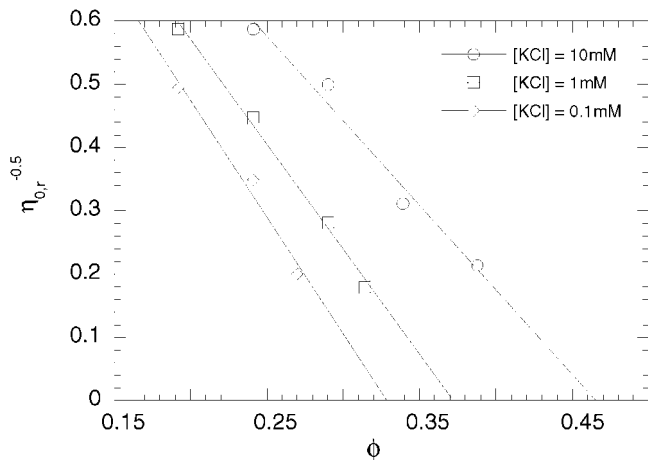


FIG. 2. Determination of ϕ_{\max} from the relative zero shear viscosity for PS200 at different salt content.

corresponding effective hard-sphere volume fraction is given in Eq. [6]:

$$a_{\text{eff}} = \left(\frac{\phi_{\max, \text{HS}}}{\phi_{\max, \text{exp}}} \right)^{1/3} \quad [5]$$

$$\phi_{\text{eff}} = \phi \cdot \left(\frac{\phi_{\max, \text{HS}}}{\phi_{\max, \text{exp}}} \right). \quad [6]$$

By rescaling the volume fraction by ϕ/ϕ_{\max} one obtains a master curve for zero-shear viscosity vs volume fraction, which validates the scaling procedure. The mastercurve is displayed in Fig. 3. The Quemada equation (Eq. [4]) is also plotted but does not describe the viscosity data for the entire range of volume fractions accurately. The deviation, which suggests that the viscosity diverges more rapidly than predicted, is opposite to that observed for soft-sphere dispersions stabilized by polymers

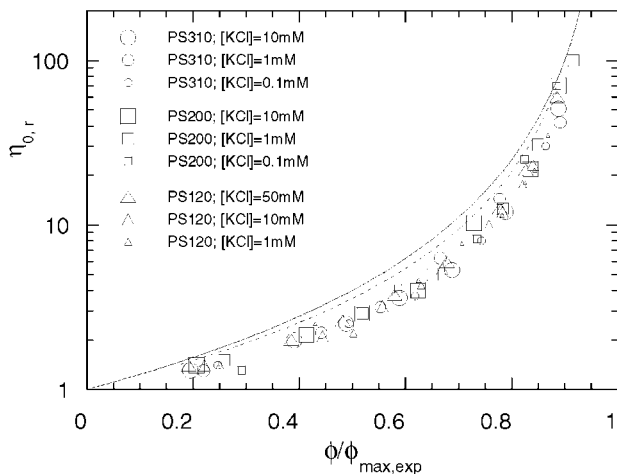


FIG. 3. Master curve for the relative zero shear viscosity η_0/μ for all samples. The line was calculated using Quemada's equation (Eq. [4]). The dotted line represents data for hard-sphere-like systems from Ref. (45).

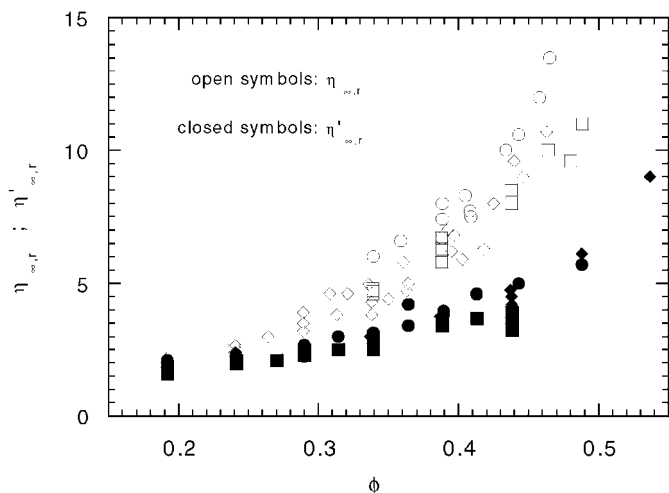


FIG. 4. Comparison of relative high shear viscosity $\eta_{\infty, r} = \eta_{\infty} / \mu$ (open symbols) and $\eta'_{\infty, r} = \eta'_{\infty} / \mu$ (closed symbols) for Latex PS120 (\circ , \bullet), PS200 (\square , \blacksquare) and PS310 (\diamond , \blacklozenge).

(44) and is more typical of hard-sphere colloids. For comparison the data for hard-sphere-like systems of Meeker *et al.* (45) was parametrized in the same way and also displayed in Fig. 3.

3.2. Viscosity and Particle Mobility

3.2.1. Comparison of high-frequency viscosity and steady shear viscosity. In Fig. 4 relative high-shear viscosity η_{∞}/μ and relative high-frequency viscosity are plotted vs volume fraction. Both quantities are independent of ionic strength, showing that direct particle interactions play a minor role in both cases. In accordance with results from hard-sphere systems investigated by van der Werff *et al.* (5) these quantities deviate from each other. The high-shear viscosity is always greater than the high-frequency viscosity. This deviation increases with increasing volume fraction. In contrast to high-frequency oscillations, high shear rates distort the dispersion microstructure significantly away from equilibrium (17). Shear forces push particles together along the compressional axis, leading to particle clustering which generates large hydrodynamic stresses (46, 47). The resulting hydrodynamic viscosity increases with shear rate, from η'_{∞} at small shear rates to larger values at the high-shear plateau (48, 49).

3.2.2. Comparison of η'_{∞} and D_s^s —Elucidating the Stokes-Einstein equation. Results for the dependence of D_s^s and η'_{∞} on volume fraction ϕ are shown in Figs. 5 and 6. D_s^s and η'_{∞} were normalized by the diffusion constant at infinite dilution, D_0 , and the solvent viscosity, μ , respectively. For all particle sizes there is no significant trend for η'_{∞}/μ with respect to different salt contents of the dispersions. The concentration dependence of η'_{∞}/μ for different electrolyte contents is the same within the accuracy of the technique. A similar behavior can be observed for the concentration dependence of the short-time self-diffusion D_s^s for PS200 and PS310; D_s^s/D_0 also does not depend on the salt content.

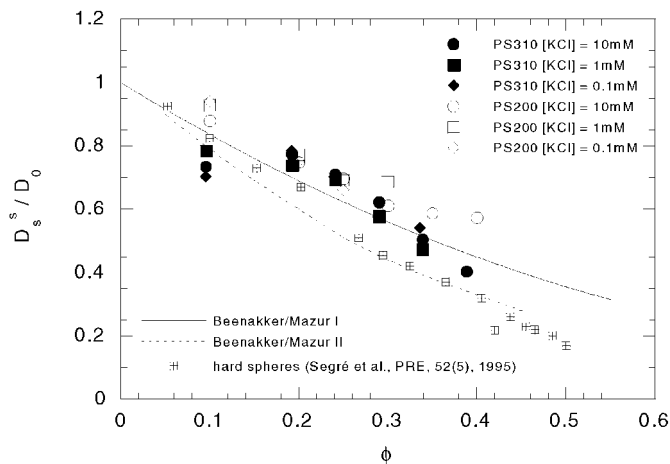


FIG. 5. Comparison of normalized short-time self-diffusion D_s^s of the charge stabilized PS-latices with hard-sphere theories for D_s^s by Beenakker and Mazur, I, (64); II, (14). Also plotted are experimental results for hard-sphere-like PMMA dispersions (50).

The observation that these dynamic suspension properties do not depend on the added electrolyte concentration, and thus are seemingly independent of the details of the interparticle potential, suggests that they may be compared directly with theories developed for hard-sphere dispersions, such as those by Beenakker (6, 14). As a first comparison, we show in Fig. 5 that our data fall on the earlier prediction of Beenakker, but above the more sophisticated prediction that includes higher order hydrodynamic interactions. To first order our data on the different sizes and salt concentrations depend on the volume fraction in the same manner as the hard-sphere data. The fact that our measured diffusivities are *slightly higher* than those measured by Segré *et al.* (50) is indeed to be expected; the finite range of the electrostatic repulsion forces the average nearest neighbor distance to be larger than that found in a true hard-sphere system.

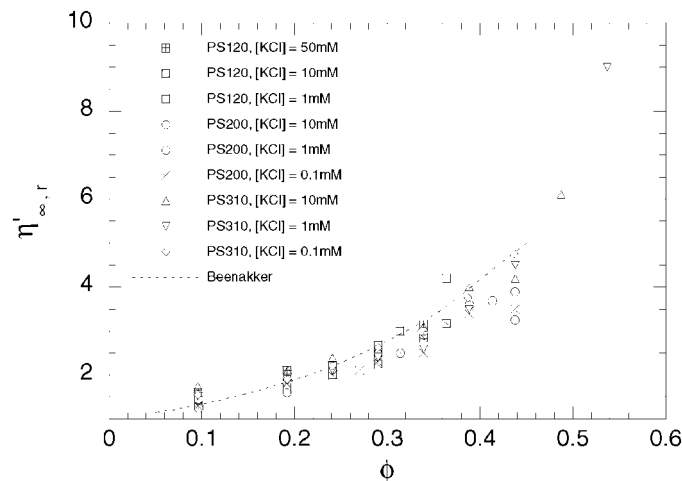


FIG. 6. $\eta_{\infty,r}$ for all samples vs volume fraction. The solid line represents the Beenakker theory (6) (see Ref. (25) for single plots for each sample).

As the lubrication part of the hydrodynamic interaction diverges as one over the separation distance between neighboring sphere surfaces, small differences in the nearest neighbor distribution will be magnified in the hydrodynamic drag on a tracer sphere diffusing in the dispersion.

We turn our attention now to the high-frequency viscosity shown in Fig. 6. Data for η'_{∞}/μ also fall onto a master curve but this curve is well described by the calculated curve of Beenakker for hard spheres that accounts for many-body hydrodynamic interactions (6). The results also agree well with η'_{∞}/μ data for hard-sphere systems measured by van der Werff *et al.* (5). Thus to within experimental resolution, the high-frequency viscosity of the charge stabilized dispersions examined here shows the same concentration dependence as hard-sphere systems. This result is consistent with previous studies (46) where the hydrodynamic interactions are found not to be overly sensitive to interparticle structure until particles are pushed into close proximity, such that lubrication forces become significant. This relative insensitivity to the details of the nearest neighbor distribution is a direct consequence of η'_{∞} being dominated by long-range, mean-field contributions to the hydrodynamic dissipation. Indeed, these results showing that η'_{∞}/μ is only a function of the volume fraction for stable lattices suggests that such measurements could be used to determine particle concentration.

In agreement with the predictions of Beenakker (6) and the exact numerical simulations of Ladd (16) for hard spheres and as noted previously (25) for charge-stabilized spheres, the generalized Stokes–Einstein relation between short-time self-diffusion and high-frequency viscosity at finite concentration (Eq. [1]) is not expected to be valid for colloidal dispersions in the presence of hydrodynamic interactions. Figure 7 displays a direct comparison that highlights the essential differences between these two properties dominated by hydrodynamic interactions. If the generalized Stokes–Einstein relation holds,

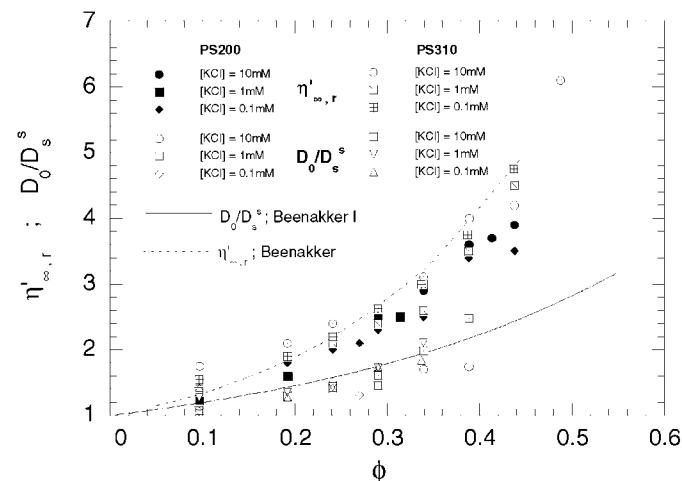


FIG. 7. Comparison of normalized high-frequency viscosity $\eta'_{\infty,r} = \eta'_{\infty}/\mu$ and short-time self-diffusion D_0/D_s^s for all samples. The lines represent theoretical predictions for $\eta'_{\infty,r}$ (dashed, (6)) and D_s^s (solid, (64)), respectively.

the curves for η'_{∞}/μ and D_s^s/D_0 should fall on a single curve. Note that η'_{∞}/μ and D_0/D_s^s coincide at low concentration, as they must, but that η'_{∞}/μ is significantly higher than D_0/D_s^s at high-volume fractions. With increasing volume fraction the deviation increases. This clearly shows that a generalized Stokes–Einstein relation does not hold for the concentrated charge-stabilized dispersions probed here. Furthermore, the deviation is in the direction expected for hard-sphere-like particles and is magnified by the excluded volume induced by the finite range of the electrostatic repulsion.

In summary, we observe a behavior that is consistent with our understanding that in stable dispersions, the high-frequency viscosity is dominated by long-range, mean field effects, whereas the short-time self-diffusivity is more sensitive to hydrodynamic interactions with the nearest neighbors. Consequently, for stable dispersion at rest, D_s^s is sensitive to the arrangement of neighboring particles and hence more sensitive to the nature of the stabilizing forces. This difference is responsible for the ability of the hard-sphere model to correctly predict η'_{∞} and yet incorrectly underestimate D_s^s for these charge stabilized latices.

3.3. Elastic Modulus and Interparticle Interactions

G'_{∞} for the samples PS120 and PS200 at volume fractions below the liquid–solid transition were also obtained using the torsional resonator. The elastic moduli of the large particle suspensions were too low for accurate measurements (note that the elastic modulus scales inversely with particle size cubed, such that viscous effects dominate the frequency response of large particle dispersions). Dispersions at volume fractions $\phi > \phi_{\max, \text{exp}}$, which were also visibly crystalline, did show viscoelastic behavior also at low frequencies. Elastic moduli were determined by means of a controlled stress rheometer (Bohlin CVO) in oscillatory shear mode over a frequency range of 0.01 to 20 Hz. The storage modulus G' increased with increasing frequency, eventually reaching an apparent plateau, as shown in Fig. 8. This

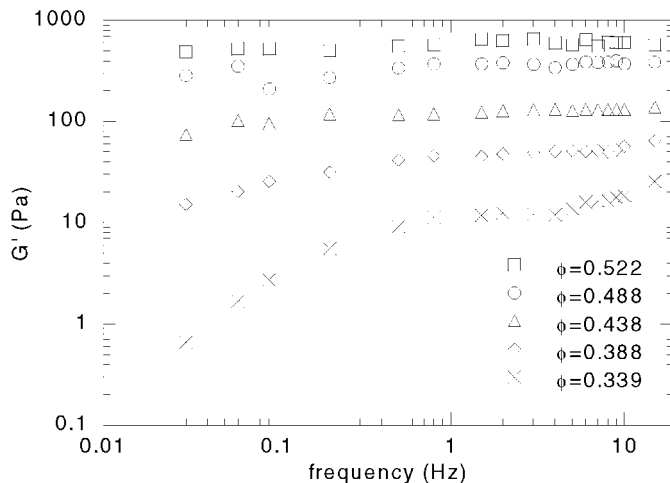


FIG. 8. Frequency dependence of G' for PS200 at $[\text{KCl}] = 0.1 \text{ mM}$ and different volume fractions.

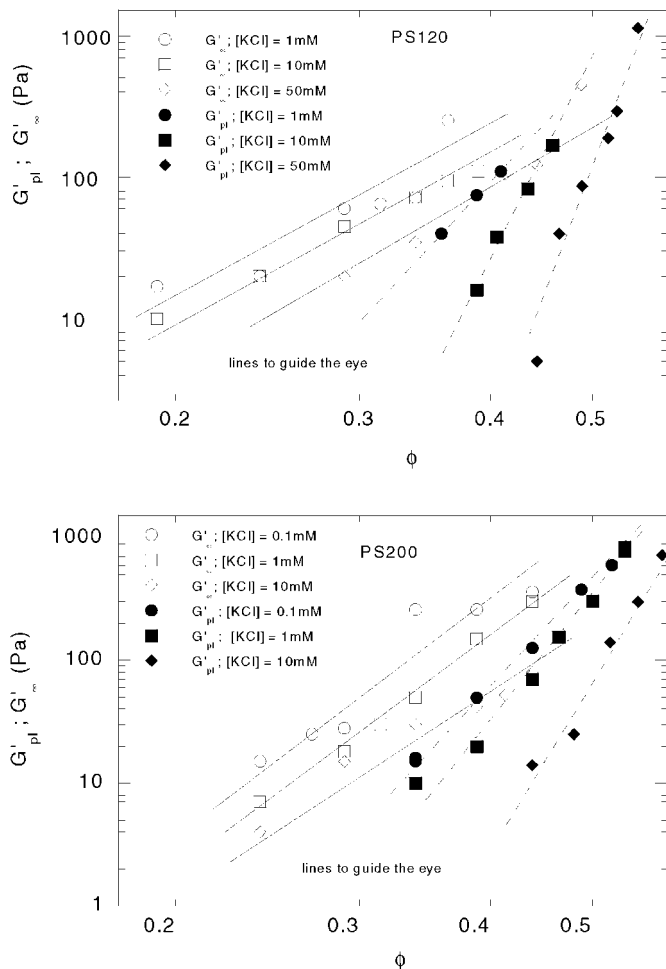


FIG. 9. G'_{∞} and G'_{pl} for PS120 (top) and PS200 (bottom) at different salt content. The filled symbols denote G'_{pl} measured in the crystalline regime of the dispersions. Lines are to guide the eye.

plateau modulus is assigned as G'_{pl} , for comparison to the values of G'_{∞} as determined from torsional resonance oscillation. We note that many investigators assume that $G'_{\infty} = G'_{\text{pl}}$ for use in determining the interaction potential from the formula for G'_{∞} .

In Fig. 9 G'_{pl} and G'_{∞} are shown as a function of volume fraction. Obviously, $G'_{\infty} > G'_{\text{pl}}$, over the volume fraction range for which both measurements were possible, for all the systems probed. It has been shown previously (23) that our resonator operates in the true high-frequency limit for particles even smaller than those probed here. Although the difference evident in Fig. 9 is not surprising as G'_{pl} is measured at frequencies much lower than those required to exceed the time scale for Brownian motion, presented here is perhaps the first, direct evidence that, at least for charge stabilized systems, the plateau values of the elastic modulus determined in a conventional rheometer greatly underestimates the true, high-frequency limiting modulus. We also observe that the volume fraction dependence of G'_{pl} is much stronger than for G'_{∞} , which is consistent with the hypothesis that rotational rheometry operates below the true limiting

frequency. At the highest volume fractions where the dispersions are the most elastic, G'_{pl} approaches what one would expect from extrapolating G'_{∞} . Also, note that both G'_{∞} and G'_{pl} are strongly influenced by the solution salt concentration. As expected, the moduli increase with increasing κ^{-1} .

3.4. Extracting Colloidal Surface Charge

An effective surface charge was extracted from the G'_{∞} data using a theory described recently by Bergenholtz *et al.* (23). The relationship between the high-frequency modulus and the interaction potential is deduced from the well-known Zwanzig and Mountain formula [7] neglecting hydrodynamic interactions (51),

$$G'_{\infty} \frac{a^3}{kT} = \frac{3\phi}{4\pi} + \frac{3\phi^2}{40\pi} \int_0^{\infty} dr g(r) \frac{d}{dr} \left(r^4 \frac{d\Psi(r)/kT}{dr} \right), \quad [7]$$

where $g(r)$ denotes the radial distribution function and $\Psi(r)$ the interaction potential between the particles. As evidenced by recent computer simulations of Bossis *et al.* (52) and a scaling analysis by Lionberger and Russel (9, 53) hydrodynamic contributions to G'_{∞} mainly occur in the lubrication zone near the particle surface and, since electrostatic repulsion keeps particles apart from this zone, neglecting hydrodynamic contributions to G'_{∞} is an admissible approximation. The radial distribution function $g(r)$ appearing in Eq. [7] depends on the surface potential of the particles, which greatly complicates a rigorous inversion of Eq. [7] to obtain the pair potential from G'_{∞} measurements. To circumvent the need for an exact calculation of $g(r)$ for charge stabilized spheres, a simplified perturbation model was proposed by Bergenholtz *et al.* (23). Assuming that only interactions with the nearest neighbor particles contribute to the elasticity and taking into account the disordered structure of the noncrystalline dispersions one obtains for thin double layers:

$$G'_{\infty} \frac{a^3}{kT} = \frac{3\phi}{4\pi} + \frac{3\phi^2}{40\pi} (2 \cdot a_{\text{eff}})^4 g_{\text{hs}}(2; \phi_{\text{eff}}) \cdot \left(-\frac{d\Psi(r)/kT}{dr} \right) \Big|_{r=2 \cdot a_{\text{eff}}}. \quad [8]$$

In Eq. [8] the structure of the true charged sphere dispersion is mapped onto the structure of a dispersion of hard spheres with diameter $2a_{\text{eff}}$ which is characterized by the pair distribution function g_{hs} . The effective hard-sphere diameter accounts for the excluded volume due to the electrostatic repulsive interaction. Equation [8] is evaluated at $r = 2a_{\text{eff}}$, i.e., at contact for the effective hard spheres.

Here we have determined a_{eff} from measurements of the zero-shear viscosity as defined in Eqs. [5] and [6]. We note that other methods for determining the effective hard-sphere diameter, such as by matching the second virial coefficients for example, are possible. However, the excellent reduction of the zero-shear rheology data to a master curve (Fig. 3) based on the effective

hard-sphere diameter determined in this manner suggests that the method is robust and accurate.

The hard-sphere radial distribution function at contact was calculated by using the Carnahan–Starling (54) expression. For volume fractions $\phi > 0.5$ a divergent form was taken, being in accordance with results for computer simulations for disordered HS dispersions.

$$g_{\text{hs}}(2; \phi) = \begin{cases} \frac{1 - \phi/2}{(1 - \phi)^3} & 0 < \phi < 0.5 \\ \frac{1}{4\phi} \frac{1.21 + \phi}{0.64 - \phi} & 0.5 < \phi < 0.64 \end{cases}. \quad [9]$$

To provide a robust and simple method of extracting a meaningful measure of surface charge from the measurements, we assume that the pair interaction potential appearing in Eq. [7] is given by a DLVO potential using a simple superposition of the Debye–Hückel solution of the linearized Poisson–Boltzmann equation as

$$\Psi(r)_{\text{DLVO}} = \frac{Q^2 \cdot L_B}{r \cdot (1 + \kappa \cdot a)^2} \cdot \exp\left(-\kappa \cdot a \cdot \left(\frac{r}{a} - 2\right)\right) - \frac{A_H}{6kT} \cdot \left(\frac{2}{\left(\frac{r}{a}\right)^2 - 4} + \frac{2}{\left(\frac{r}{a}\right)^2} + \ln\left(\frac{\left(\frac{r}{a}\right)^2 - 4}{\left(\frac{r}{a}\right)^2}\right) \right). \quad [10]$$

In Eq. [10], Q is the number of effective surface charges per particle, $L_B = e^2/(4\pi\epsilon_0\epsilon_r kT)$ (Bjerrum-length), A_H is the Hamaker constant (PS/water: $A_H = 1.3 \times 10^{-20}$ J), a is the radius of particle, and r is the distance between particle centers. Recognizing that this choice of electrostatic potential is an approximation, we will treat the surface charge determined via this method as an *effective* surface charge; the consequences of this approximation will be explored shortly.

Given the above relations, measurements of the colloid size, Hamaker constant, and solution ionic strength serve to characterize the potential except for knowledge of the surface charge. Zero shear viscosity measurements yield the effective hard-sphere mapping that then enables using Eqs. [9] and [10] to deduce the surface potential directly from a single measurement of the high-frequency elastic modulus. In practice, however, it is more accurate and reliable to fit an entire concentration series to a single value of surface charge, as shown in Fig. 10. Furthermore, we note that by assuming the linear superposition of the Debye–Hückel form of the electrostatic potential, which is the solution of the linearized Poisson–Boltzmann equation, we are clearly determining an *effective* surface charge. Previous work by Alexander *et al.* (55) and Löwen and Kramposthuber (56) support this procedure as being robust and provide guidance as to methods of renormalizing this effective surface charge into a true surface charge. The renormalization accounts for the fact that our choice of potential does not account for the full nonlinearities of the double-layer potential, but is an exact solution at relatively large separation distances if one takes the surface charge to be an effective surface charge.

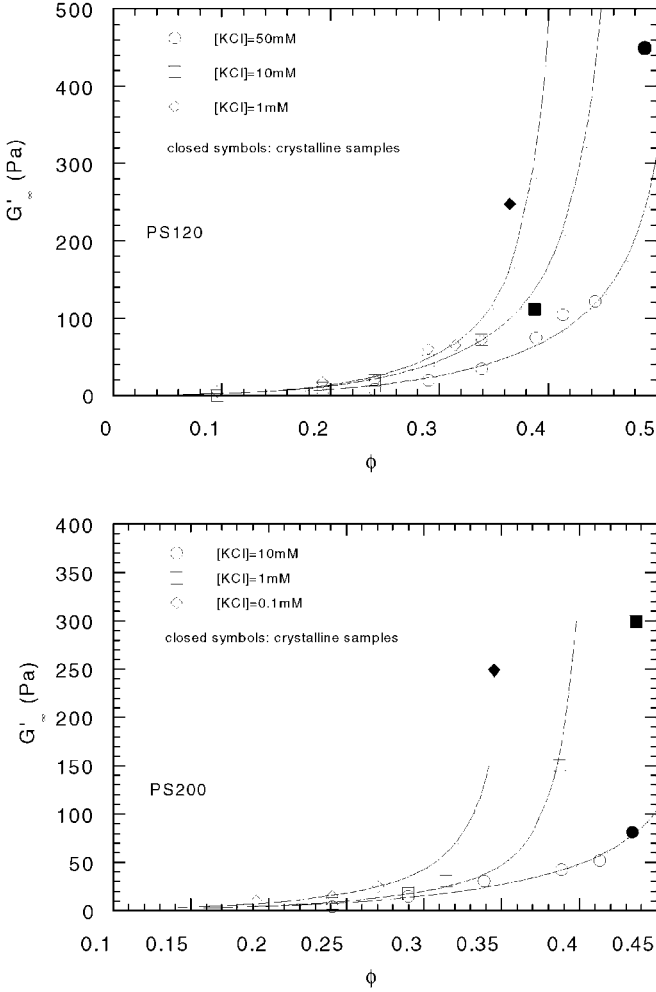


FIG. 10. G'_∞ for PS120 (top) and PS200 (bottom) at different salt contents plotted vs volume fraction of the PS. The lines represent fits to G'_∞ data obtained by the variation of the surface charge according to Bergenholtz *et al.* (23) ($\phi_{\max,HS} = 0.58$ was used in fitting procedure). Filled symbols correspond to crystalline samples; these data were not used in the fitting procedure.

The values of ϕ_{eff} were calculated by using Eq. [6] and taking $\phi_{\max,HS}$ to lie on the range 0.58 to 0.63 defined by experimental results for hard-sphere systems reported by Marshall and Zukoski (57) and Buscall *et al.* (58). We note that, as with the previous work, the fit results for the potential are sensitive to the value of $\phi_{\max,HS}$, we take $\phi_{\max,HS} = 0.58$ to calculate the value of ϕ_{eff} and report the surface charge determined using this value in Table 4. This $\phi_{\max,HS}$ value is consistent with the most recent measurements for monodisperse hard-sphere systems that show divergence of η_0 at the glass transition ($\phi = 0.58$) (45, 59). To convert these effective surface charges to surface potentials, we use the following relationship:

$$\frac{Q}{a} = (1 + \kappa a) \frac{e\Psi_s}{kT}. \quad [11]$$

The results for the effective surface charge depend on the choice of $\phi_{\max,HS}$ for the hard-sphere system, as can be seen

from the data summarized in Table 4, where the values are given for $\phi_{\max,HS} = 0.58$ and 0.61 (this is illustrated further below in figure 12). Not shown are the modulus fits, which are visibly worsened with increasing $\phi_{\max,HS}$ (especially at 0.63). Based on the quality of the fit theory to the measured moduli, we distinguished 0.58 as the most consistent choice within the experimentally reported range of values. Further justification for this choice of the maximum hard-sphere packing fraction comes from the agreement achieved with other, independent measures of the surface charge, to be discussed next.

Effective diameters for charged particles can also be calculated by using a perturbation theory describing the disorder-order transition for charged dispersions (60, 61). This provides a further method of determining surface charge in a concentrated dispersion. For strongly interacting particles with substantially overlapping double layers the following expression is appropriate:

$$a_{\text{eff}} \approx \frac{\kappa^{-1}}{2} \ln(\alpha / \ln(\alpha / \ln(\alpha / \dots))), \quad [12]$$

with

$$\alpha = \frac{4\pi\epsilon\epsilon_0\Psi_s^2 a^2 \kappa \exp(2a\kappa)}{kT}.$$

Assuming that a_{eff} appearing in Eq. [12] can be equated to the value of a_{eff} previously determined from the divergence of the low-shear viscosity (see Fig. 2 and Eq. [5]), we calculate the surface potentials reported in Table 4.

Despite the fact that Eq. [12] was derived for low ionic strengths, results for the effective surface potentials extracted from both high-frequency and low-shear experiments are in remarkable agreement. They exhibit a similar dependence on salt content and both quantities are in good quantitative agreement. This result suggests that for the lattices probed here, a simple measurement of the maximum packing fraction from low-shear rheology suffices to determine the effective surface charge. Whether this is coincidence or a robust result requires a more thorough exploration that is beyond the scope of this paper.

Finally, we note that the determination of the critical coagulation concentration (ccc) can be used to estimate the surface charge by assuming a Hamaker constant for the PS particles. The measured concentration of KCl required to flocculate diluted latex samples was input into the calculation of the DLVO-potential and ψ_s was varied until the maximum of the potential curve reached zero. The experimental determination of the ccc is inherently imprecise, requiring a judgement of when rapid flocculation is actually achieved. However, setting the stability criterion to a few kT did not change the results significantly. Our estimates of the surface potential from ccc measurements are also given in Table 4.

Previous work has attempted to extract surface charge from measurements of the plateau modulus as determined from rotational rheometry at lower frequencies. Analogously, G'_{pl} was determined and used to calculate the surface charge by a model

TABLE 4
Results for Determination of the Effective Surface Charge (Q) and Surface Potentials (ψ_s) from the Different Methods

	κa	Q (e) from G'_∞)	ψ_s (mV) from G'_∞)	ψ_s (mV) from G'_{pl})	ψ_s (mV from Pertub. Theory)	ψ_s (mV from ccc)	ψ_s (mV from ζ -pot) ^b
PS120 50 mM	44	4800	-32	-122	-38		-79
		8360	-57				
PS120 10 mM	20	1950	-28	-36	-32		-76
		2440	-38				
PS120 1 mM	6.6	320	-13	-15	-11		-64
		320	-13				
PS120 ^a			-31		-36		
			-52				
PS120						-38	
PS200 10 mM	33	7350	-38	-36	-40		-81
		11700	-62				
PS200 1 mM	10.5	1400	-22	-29	-18		-60
		1680	-26				
PS200 0.1 mM	3.5	380	-15	-60	-7		-60
		380	-15				
PS200 ^a			-37		-38		
			-58				
PS200						-35	

Note. The G'_∞ data were evaluated with $\phi_{\max,HS}$ set to 0.58 (first number) and 0.61 (second number), respectively.

^a Surface potential calculated from charge density by Debye-Hückel (see Eq. [11]).

^b ζ -Potential calculated from mobility data by Henry's equation (42).

presented by Buscall and coworkers (1, 62). As shown in Fig. 9, G'_∞ is larger than G'_{pl} . In the literature it is often assumed that $G'_\infty = G'_{pl}$ and here we explore if the surface potential extracted from the model proposed by Buscall *et al.* for G'_{pl} is consistent with the other methods. This model requires samples with solid-like structure, indicated by a finite low-shear modulus and an infinite value for η_0 . It was shown that the model proposed by Buscall *et al.* is not applicable to G'_∞ data and the relationship of the modulus at low frequencies to the high-frequency modulus has been previously discussed by Wagner (28).

Assuming a fcc lattice the theoretical elastic modulus $G'_{pl,theo}$ was calculated according to Eq. [13] as a function of volume fraction, salt content, and surface potential. Interparticle forces were calculated neglecting van der Waals attractions:

$$G'_{pl,theo} = \frac{2\pi\alpha\epsilon_0\epsilon_r a \Psi_s^2}{r} \left(\frac{\kappa^2 \exp(-\kappa(r-2a))}{(1 + \exp(-\kappa(r-2a)))^2} \right), \quad [13]$$

with

$$\alpha = \left(\frac{1}{5\pi} \right) \Phi_m N$$

and r denoting the particle distance ($r = 2a \cdot (\phi_{\max}/\phi)^{1/3}$); for fcc packing, ϕ_{\max} is set to 0.74 and $N = 12$.

In Fig. 11 G'_{pl} is plotted vs $G'_{pl,theo}/\Psi_s^2$ and the slope of the linear least square fit yields the surface potential. The results for the surface potentials are listed in Table 4. Notice that there is curvature in the data that cannot be captured by the model.

3.5. Comparison of Results

Table 4 summarizes the surface potential determined via the different methods. Results from G'_∞ and perturbation theory ($\phi_{\max,exp}$) are comparable and yield the same dependence on added salt. The results for ψ_s determined from critical coagulation concentration measurements correspond favorably well with results from the high frequency modulus measured in concentrated dispersion, but are much lower than the ζ -potentials determined from electrophoretic measurements of diluted lattices. This indicates that results for the effective surface charge

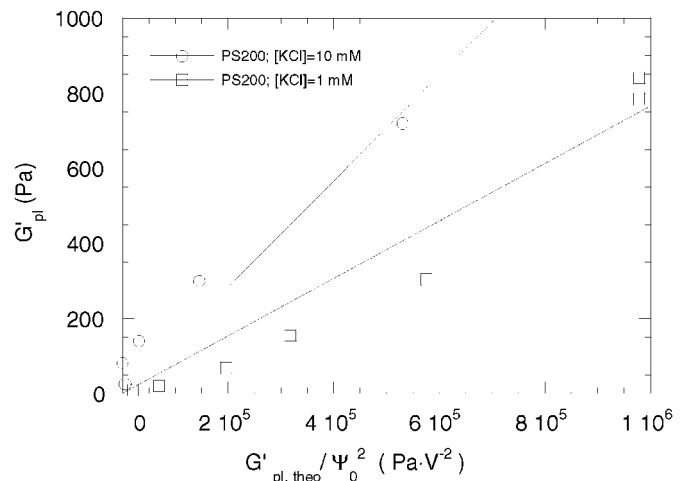


FIG. 11. Evaluation of the low-frequency plateau modulus G'_{pl} obtained from crystalline samples according to the model by Buscall *et al.* (62).

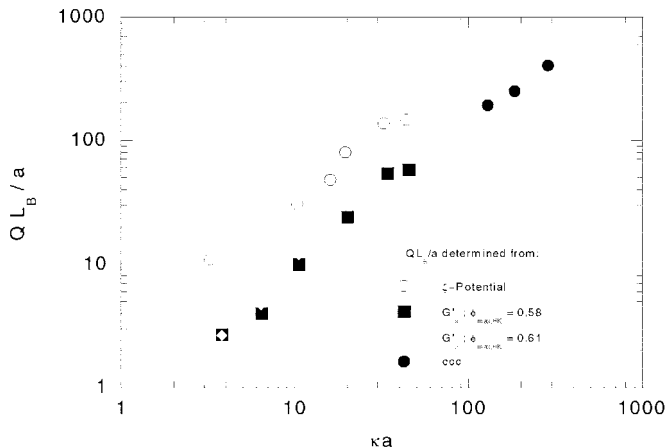


FIG. 12. Surface charge density vs κa for all samples, as determined from electrophoretic mobility, ccc, and from the elastic moduli. For the latter the variation with the value of the maximum hard sphere packing fraction is shown for comparison.

determined by torsional high frequency measurements are more reliable predictions for the salt stability of charge-stabilized dispersions than ζ -potentials determined from electrophoretic mobilities.

The evaluation of the low-frequency plateau modulus according to the model proposed by Buscall *et al.* leads to an agreement with results from high-frequency and ccc data only in some cases. Large deviations are found at both high and low salt content, such that the deviations cannot be anticipated. Hence, we conclude that this approach cannot be used consistently to accurately determine surface potentials under all conditions.

In Fig. 12 we replot the results for the surface charge determination from the high-frequency torsional resonance (shown for data evaluation with $\phi_{\max,HS} = 0.58$ and 0.61 , respectively), ccc measurements, and electrophoretic mobilities as suggested by the Debye–Hückel formula (Eq. [11]). The surface charge determined from electrophoresis is a linear function of the dimensionless inverse Debye length, but is higher than that determined from the other two methods. Notice that in Fig. 12, all the results for the different salt concentrations, colloid concentrations, and particle sizes are compared. The effective charge data calculated from the the high-frequency modulus and those determined from the ccc measurements appear to fall along one curve when $\phi_{\max,HS} = 0.58$ is considered, suggesting that the high-frequency measurements are a better prediction of the salt stability of these latices. Note, however, that the data trace out a sigmoidal curve, which is not consistent with a unique value of surface potential independent of salt concentration. The more rapid increase in surface charge with increasing salt concentration (increasing $\kappa \cdot a$) would be typical of a charge regulation mechanism, whereby added salt increases the dissociation of a weak acid on the colloid surface. However, the model system here contains only strong acid groups on the surface and the pH is far from the pK_a of the sulfonate surface acid groups; hence this mechanism is not applicable for our model colloids. A possible mechanism for this nonlinear increase of surface charge

with added salt is counterion condensation near the particle surface, which would lower the surface potential and result in an effective surface charge that would be an increasing function of the ionic strength (63).

4. CONCLUSIONS

The purpose of this work was to explore the hydrodynamic and colloidal interactions in a model, concentrated, charge-stabilized colloidal dispersion using rheological and light scattering techniques. Particular emphasis was placed on interpreting the dependence of rheological and dynamical properties on salt content, particle size, and volume fraction in terms of hard-sphere scaling laws.

- Comparisons of η'_∞ and η_∞ show that although both are dominated by hydrodynamic interactions, as evidenced by their insensitivity to particle size and salt concentration, η'_∞ is smaller than η_∞ . This can be traced to the shear distortion of the microstructure, such that the extended Cox–Merz rule will not apply to these fluids.

- The high-frequency viscosity η'_∞ is well represented by the theory for hard spheres, illustrating how insensitive this property is to interparticle interactions in stable dispersions and suggesting a robust method of determining particle concentration in stable, concentrated dispersions.

- D_s^s is also insensitive to interparticle interactions, as evidenced by independence on salt concentration and particle size. D_s^s to first order does follow the Beenakker theory for hard spheres, but slight systematic deviations to faster diffusion are observed. This might be traced back to the electrostatic repulsion preventing close approach of the colloids and reducing lubrication contributions to the hydrodynamic drag.

- Comparison of η'_∞ to $1/D_s^s$ illustrates the violation of the generalized Stokes–Einstein relationship as already predicted for hard-sphere dispersions (6).

- G'_{pl} measured by low-frequency rotational rheometry underestimates the true G'_∞ as determined by high-frequency torsional resonance oscillation.

- The apparent colloidal surface charge can be extracted from G'_∞ measurements and is in good agreement with results from ccc measurements when $\phi_{\max,HS}$ was set to 0.58 in the fitting procedure for the G'_∞ data. This $\phi_{\max,HS}$ value is consistent with the most recent measurements for monodisperse hard-sphere systems that show divergence of η_0 at the glass transition ($\phi = 0.58$) (45, 59).

- Electrophoretic mobility measurements overestimate the surface potential as compared to all the other methods. The reasons for this discrepancy are not understood. This stands in contrast to previous measurements on a different latex (see Ref. (23)), where congruence between methods was found.

ACKNOWLEDGMENTS

F.M.H. and W.R. thank the BMBF (Grant 03D0039D7) and the Deutsche Forschungsgemeinschaft for financial support. N.J.W. acknowledges support from the NSF (Grant CTS-9523968) and the Fulbright Commission for a Senior

Scholar Fellowship. Discussions with G. Nägele and R. Klein of the University of Konstanz are gratefully acknowledged.

REFERENCES

- Buscall, R., *J. Chem. Soc. Faraday Trans.* **87**, 1365 (1991).
- Buscall, R., *Colloids Surf. A* **83**, 33 (1994).
- Wagner, N. J., and Klein, R., *Colloid Polym. Sci.* **269**, 295 (1991).
- Brady, J. F., *J. Chem. Phys.* **99**, 567 (1993).
- Werff, J. C. V. D., Kruif, C. G. D., Blom, C., and Mellema, J., *Phys. Rev. A* **39**, 795 (1989).
- Beenakker, C. W. J., *Physica* **128**, 48 (1984).
- Blom, C., Mellema, J., Lopulissa, J. S., and Reuvers, A. J., *Colloid Polym. Sci.* **262**, 397 (1984).
- Shikata, T., and Pearson, D. S., *J. Rheol.* **38**, 601 (1994).
- Lionberger, R. A., and Russel, W. B., *J. Rheol.* **38**, 1885 (1994).
- Gisler, T., and Weitz, D. A., *Curr. Opin. Colloid Interface Sci.* **3**, 586 (1998).
- Imhof, A., Blaaderen, A. V., Maret, G., Mellema, J., and Dhont, J. K. G., *J. Chem. Phys.* **100**, 2170 (1994).
- Segré, P. N., Meeker, S. P., Pusey, P. N., and Poon, W. C. K., *Phys. Rev. Lett.* **75**, 958 (1995).
- Banchio, A. J., Bergenholtz, J., and Naeyegele, G., *Phys. Rev. Lett.* **82**, 1792 (1999).
- Beenakker, C. W. J., and Mazur, P., *Physica* **126**, 349 (1984).
- Phillips, R. J., Brady, J. F., and Bossis, G., *Phys. Fluids* **31**, 3462 (1988).
- Ladd, A. J. C., *J. Chem. Phys.* **93**, 3484 (1990).
- Batchelor, G. K., and Green, J. T., *J. Fluid Mech.* **56**, 401 (1972).
- Batchelor, G. K., *J. Fluid Mech.* **74**, 1 (1976).
- Cichocki, B., and Felderhof, B. U., *J. Chem. Phys.* **89**, 1049 (1988).
- Zhu, J. K., Durian, D. J., Müller, J., Weitz, D. A., and Pine, D. J., *Phys. Rev. Lett.* **68**, 2559 (1992).
- Lilge, D., and Horn, D., *Colloid Polym. Sci.* **269**, 704 (1991).
- Wiese, H., and Horn, D., *J. Chem. Phys.* **94**, 6429 (1991).
- Bergenholtz, J., Willenbacher, N., Wagner, N. J., Morrison, B., van den Ende, D., and Mellema, J., *J. Colloid Interface Sci.* **202**, 430 (1998).
- Wagner, N. J., *Curr. Opin. Colloid Interface Sci.* **3**, 391 (1998).
- Bergenholtz, J., Horn, F. M., Richterling, W., Willenbacher, N., and Wagner, N. J., *Phys. Rev. E* **58**, 4088 (1998).
- Buscall, R., Goodwin, J. W., Hawkins, M. W., and Ottewill, R. H., *J. Chem. Soc. Faraday Trans. 1* **78**, 2873 (1982).
- Goodwin, W., and Ottewill, R. H., *J. Chem. Soc. Faraday Trans. 2* **87**, 357 (1991).
- Wagner, N. J., *J. Colloid Interface Sci.* **161**, 169 (1993).
- Koppel, D. E., *J. Chem. Phys.* **57**, 4814 (1972).
- Wiese, H., and Horn, D., *Ber. Bunsenges. Phys. Chem.* **96**, 1818 (1992).
- Pusey, P. N., and Tough, R. J. A., "Dynamic Light Scattering." Plenum, New York, 1985.
- Nägele, G., *Phys. Rep.* **272**, 215 (1996).
- Pusey, P. N., "Liquids, Freezing, and Glass Transition." Elsevier, North-Holland/Amsterdam, 1991.
- Frith, W. J., Strivens, T. A., and Mewis, J., *J. Colloid Interface Sci.* **139**, 55 (1990).
- Stone-Masui, J., and Watillon, A., *J. Colloid Interface Sci.* **52**, 479 (1975).
- Tuin, G., Senders, J. H. J. E., and Stein, H. N., *J. Colloid Interface Sci.* **179**, 522 (1996).
- Kolthoff, I. M., and Miller, I. K., *J. Am. Chem. Soc.* **73**, 3055 (1951).
- Antonietti, M., and Vorwerg, L., *Colloid Polym. Sci.* **275**, 883 (1997).
- Verdegan, B. M., and Anderson, M. A., *J. Colloid Interface Sci.* **158**, 372 (1993).
- Chow, R. S., and Takamura, K. J., *J. Colloid Interface Sci.* **125**, 226 (1988).
- O'Brien, R. W., and White, L. R., *J. Chem. Soc. Faraday Trans. 2* **74**, 1607 (1978).
- Henry, D. C., *Proc. R. Soc. London A* **133**, 106 (1931).
- Quemada, D., *Rheol. ACTA* **16**, 82 (1977).
- Maranzano, B., and Wagner, N. J., *Rheol. Acta*, submitted for publication.
- Meeker, S. P., Poon, W. C. K., and Pusey, P. N., *Phys. Rev. E* **55**, 5718 (1997).
- Bender, J. W., and Wagner, N. J., *J. Rheol.* **40**, 899 (1996).
- Phung, T. N., Brady, J. F., and Bossis, G., *J. Fluid Mech.* **313**, 181 (1996).
- Brady, J. F., and Foss, D., *J. Fluid Mech.* **401**, 243 (1999).
- Brady, J. F., and Morris, J., *J. Fluid Mech.* **348**, 103 (1997).
- Segré, P. N., Behrend, O. P., and Pusey, P. N., *Phys. Rev. E* **52**, 5070 (1995).
- Zwanzig, R., and Mountain, R. D., *J. Chem. Phys.* **43**, 4464 (1965).
- Bossis, G., Brady, J. F., and Mathis, C., *J. Colloid Interface Sci.* **126**, 1 (1988).
- Lionberger, R. A., and Russel, W. B., *J. Rheol.* **41**, 399 (1997).
- Carnahan, N. F., and Starling, K. E., *J. Chem. Phys.* **51**, 635 (1969).
- Alexander, S., Hone, D., Chaikin, P. M., Grant, P., and Morales, G. J., *J. Chem. Phys.* **80**, 5776 (1984).
- Löwen, H., and Kramposthuber, G., *Europhys. Lett.* **23**, 673 (1993).
- Marshall, L., and Zukoski, C. F., *J. Phys. Chem.* **94**, 1164 (1990).
- Buscall, R., D'Haene, P., and Mewis, J., *Langmuir* **10**, 1439 (1994).
- Phan, S.-E., Russel, W. B., Cheng, Z., Zhu, J., Chaikin, P. M., Dunsmuir, J. H., and Ottewill, R. H., *Phys. Rev. E* **54**, 6633 (1996).
- Russel, W. B., Saville, D. A., and Schowalter, W. R. "Colloidal Dispersions." Cambridge University Press, Cambridge, 1989.
- Chaikin, P. M., Pincus, P., Alexander, S., and Hone, D., *J. Colloid Interface Sci.* **89**, 555 (1982).
- Buscall, R., Goodwin, J. W., Hawkins, M. W., and Ottewill, R. H., *J. Chem. Soc. Faraday Trans. 2* **78**, 2889 (1982).
- Alexander, S., Chaikin, P. M., Grant, P., Morales, P., and Pincus, P., *J. Chem. Phys.* **80**, 5776 (1984).
- Beenakker, C. W. J., and Mazur, P., *Physica* **120**, 388 (1983).